Vibronic origin of sulfur mass-independent isotope effect in photoexcitation of SO_2 and the implications to the early earth's atmosphere

Andrew R. Whitehill[a,1], Changjian Xie[b], Xixi Hu[b], Daiqian Xie[b,1], Hua Guo[c], and Shuhei Ono[a]

[a]Department of Earth, Atmospheric, and Planetary Sciences, Massachusetts Institute of Technology, Cambridge, MA 02139; [b]Institute of Theoretical and Computational Chemistry, Key Laboratory of Mesoscopic Chemistry, School of Chemistry and Chemical Engineering, Nanjing University, Nanjing 210093, China; and [c]Department of Chemistry and Chemical Biology, University of New Mexico, Albuquerque, NM 87131

Edited by Mark H. Thiemens, University of California, San Diego, La Jolla, CA, and approved June 14, 2013 (received for review April 12, 2013)

Signatures of mass-independent isotope fractionation (MIF) are found in the oxygen (^{16}O,^{17}O,^{18}O) and sulfur (^{32}S, ^{33}S, ^{34}S, ^{36}S) isotope systems and serve as important tracers of past and present atmospheric processes. These unique isotope signatures signify the breakdown of the traditional theory of isotope fractionation, but the physical chemistry of these isotope effects remains poorly understood. We report the production of large sulfur isotope MIF, with $\Delta^{33}S$ up to 78‰ and $\Delta^{36}S$ up to 110‰, from the broadband excitation of SO_2 in the 250–350-nm absorption region. Acetylene is used to selectively trap the triplet-state SO_2 ($\tilde{a}^3B_1$), which results from intersystem crossing from the excited singlet ($\tilde{A}^1A_2/\tilde{B}^1B_1$) states. The observed MIF signature differs considerably from that predicted by isotopologue-specific absorption cross-sections of SO_2 and is insensitive to the wavelength region of excitation (above or below 300 nm), suggesting that the MIF originates not from the initial excitation of SO_2 to the singlet states but from an isotope selective spin–orbit interaction between the singlet ($\tilde{A}^1A_2/\tilde{B}^1B_1$) and triplet ($\tilde{a}^3B_1$) manifolds. Calculations based on high-level potential energy surfaces of the multiple excited states show a considerable lifetime anomaly for $^{33}SO_2$ and $^{36}SO_2$ for the low vibrational levels of the $\tilde{A}^1A_2$ state. These results demonstrate that the isotope selectivity of accidental near-resonance interactions between states is of critical importance in understanding the origin of MIF in photochemical systems.

photochemistry | sulfur dioxide | excited electronic states | absorption spectrum

Stable isotope fractionation theory predicts that the magnitude of stable isotope fractionation scales with the differences in isotopic mass (1, 2). Almost all physical, chemical, and biological processes in nature follow this mass-dependent scaling law, resulting in nearly all terrestrial materials with oxygen having $\delta^{17}O = 0.52 \times \delta^{18}O$, whereas those with sulfur have $\delta^{33}S = 0.515 \times \delta^{34}S$ and $\delta^{36}S = 1.90 \times \delta^{34}S$.[†] Significant deviations from these mass-dependent scaling laws are referred to as mass-independent fractionation (MIF), and serve as important tracers in the earth and planetary sciences (see refs. 3–5).

Early studies suggested that MIF could result only from nucleosynthetic processes (6), and the earliest measurements of oxygen MIF in calcium–aluminum inclusions of meteorites originally were interpreted to be nucleosynthetic in origin (7). It eventually was suggested (8) that chemical processes, such as tunneling or processes associated with predissociation, also might produce MIF. The first experimental evidence for a chemical origin of MIF came from ozone generated by an electric discharge or UV radiation (9, 10). The discovery of oxygen MIF in stratospheric ozone (11) soon triggered intense research into the physiochemical origin of MIF in the ozone system (see refs. 12–14). The possible chemical origins of MIF signatures still are poorly understood.

For the sulfur isotope system (^{32}S, ^{33}S, ^{34}S, and ^{36}S), Farquhar et al. (15) made the remarkable discovery that mass-independent sulfur isotope fractionation (S-MIF) is prevalent in sedimentary rocks older than *ca*. 2.4 Ga but absent in rocks from subsequent periods. The disappearance of S-MIF at about 2.4 Ga (16, 17) signifies a fundamental change in the earth's surface sulfur cycles, and generally is linked to the suppression of both SO_2 photolysis and the formation of elemental sulfur aerosols by the rise of atmospheric oxygen levels (15, 18, 19). The Archean S-MIF is considered the most compelling evidence for an anoxic early atmosphere and constrains Archean oxygen levels to be less than 10^{-5} of present levels (19). This model of oxygen evolution, however, depends critically on the assumption that UV photolysis of SO_2 by ~200 nm radiation is the ultimate source of the anomalous sulfur isotope signature (18). Constraining the source of the S-MIF requires a thorough understanding of the physiochemical origins of S-MIF during the photochemistry of SO_2.

SO_2 exhibits two strong absorption band systems in the UV region: one between 185 nm and 235 nm ($\tilde{C}^1B_2 \leftarrow \tilde{X}^1A_1$) and the other from 240 to 350 nm ($\tilde{A}^1A_2$, $\tilde{B}^1B_1 \leftarrow \tilde{X}^1A_1$) (ref. 20 and references therein); we will refer to them as the photolysis and photoexcitation bands, respectively. Excitation into the photolysis band leads to the predissociation of SO_2 into SO and O below 220 nm. Laboratory experiments by Farquhar et al. (18) showed production of large ($\Delta^{33}S$ up to 70‰) S-MIF by SO_2 photolysis using an ArF (193-nm) excimer laser source. This was used to link the high-energy photolysis band system to Archean S-MIF, and fueled subsequent detailed investigations (e.g., refs. 21–26) into the S-MIF production from photochemistry in this region. However, recent experiments (24–26) using broadband (as opposed to laser) light sources show S-MIF patterns different from the 193-nm experiments by Farquhar et al. (18). Large-magnitude ($\Delta^{33}S > 2.5‰$) MIF is produced only by experiments with high SO_2 column densities, suggesting a strong contribution from

Author contributions: A.R.W., D.X., H.G., and S.O. designed research; A.R.W., C.X., X.H., and S.O. performed research; A.R.W., C.X., X.H., D.X., H.G., and S.O. analyzed data; and A.R.W., D.X., H.G., and S.O. wrote the paper.

The authors declare no conflict of interest.

This article is a PNAS Direct Submission.

[1]To whom correspondence may be addressed. E-mail: arwhite@mit.edu or dqxie@nju.edu.cn.

This article contains supporting information online at www.pnas.org/lookup/suppl/doi:10.1073/pnas.1306979110/-/DCSupplemental.

[†]Isotope ratios are reported in δ value defined as

$$\delta^x S = {}^xR_{sa}/{}^xR_i - 1,$$

where ${}^xR$ is the ratio ${}^xS/{}^{32}S$ (x = 33, 34, or 36) of sample (R_{sa}) and initial SO_2 (R_i), respectively. For discussions of geological samples, ${}^xR_i$ is the ${}^xS/{}^{32}S$ ratio of the international sulfur isotope standard Vienna Canyon Diablo Troilite (V-CDT). These δ values are reported in tenths of a percent (‰) as convention. The capital delta notations are calculated according to

$$\Delta^{33}S = \left({}^{33}R_{sa}/{}^{33}R_i\right) \Big/ \left({}^{34}R_{sa}/{}^{34}R_i\right)^{0.515} - 1, \text{ and}$$

$$\Delta^{36}S = \left({}^{36}R_{sa}/{}^{36}R_i\right) \Big/ \left({}^{34}R_{sa}/{}^{34}R_i\right)^{1.90} - 1.$$

spectroscopic self- and mutual-shielding, although additional mechanisms also may play a role (26). The elemental sulfur products produced by these experiments are characterized by large $\delta^{34}S$ fractionations and $\Delta^{36}S/\Delta^{33}S$ ratios that differ from those observed in the Archean rock record (24–26). Discrepancies between experimental results and the geological record require a reanalysis of the origin of Archean S-MIF signatures.

SO_2 photochemistry in the photoexcitation (240–350-nm) band also has been shown to produce S-MIF (18, 25, 27, 28) and has been implicated as the source of S-MIF in stratospheric sulfate aerosols trapped in polar ice (28–31). It also has been suggested that SO_2 photochemistry in the photoexcitation band might have made secondary contributions to the S-MIF signatures during some periods of the Archean (25, 32). This band system is associated with the excitation of SO_2 into a mixed $\tilde{A}^1A_2/\tilde{B}^1B_1$ state, which also interacts with lower-lying triplet states ($\tilde{a}^3B_1$, possibly also $\tilde{b}^3A_2$) (Fig. 1) (20). Recently published absorption cross-sections of isotopically enriched SO_2 (27) in this region allow the accurate prediction of the MIF produced during the initial excitation step (28). In this study, we focus on the production of S-MIF by SO_2 excited into the photoexcitation band, and compare the results with the measured isotopologue specific cross-sections, to test the importance of chemistry after photoexcitation. Our results show a strong dependence of the S-MIF on the SO_2 and bath gas pressures but not on the detailed spectrum regions of excitation, suggesting that isotopologue selective vibronic coupling produces significant S-MIF independent of absorption cross-section differences. A theoretical model also is presented to test this hypothesis.

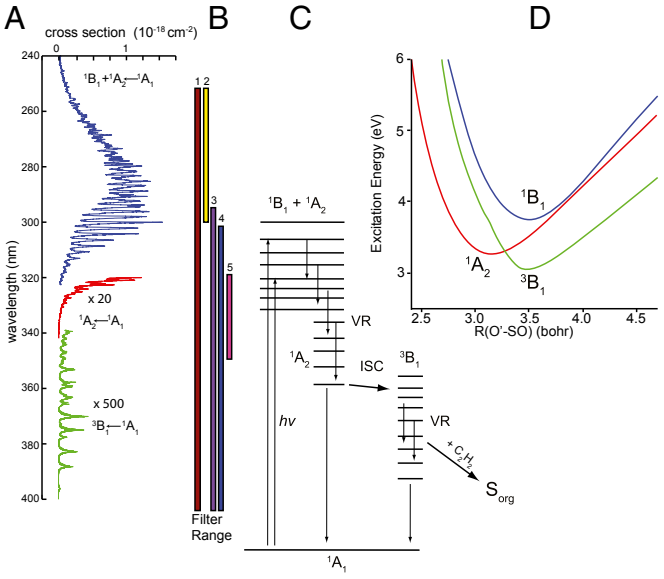

Fig. 1. Photochemistry of SO_2 in the 240–400-nm region. (*A*) UV absorption cross-section for SO_2 between 240 and 400 nm (from refs. 33 and 34). (*B*) Vertical lines showing the spectral ranges for the different optical filters tested. (*C*) Schematic of the photochemistry of the experiments. SO_2 initially is excited into the coupled $\tilde{B}^1B_1/\tilde{A}^1A_2$ states. It vibrationally relaxes (VR) via collisions with the bath gas. At low vibrational levels of the $\tilde{A}^1A_2$ state, intersystem crossing may lead to irreversible crossing to the $\tilde{a}^3B_1$ state as the result of vibrational relaxation of the $\tilde{a}^3B_1$ state below the origin of the $\tilde{A}^1A_2$ band. Isotope effects due to near-resonant spin–orbit coupling between the singlet and triplet states in this region may lead to mass-independent isotope anomalies in the resulting triplet-state SO_2. The triplet-state SO_2 finally reacts with acetylene (C_2H_2) to form the organosulfur products analyzed in this study. (*D*) Potential energy surfaces for the singlet and triplet states of SO_2 as a function of the O′-SO Jacobi distance with the S-O distance and the Jacobi angle optimized.

Methods

A series of SO_2 photochemical experiments were carried out using a flow-through photochemical system to investigate S-MIF signatures as a function of SO_2 [0.1–10 millibars (mbar)] and nitrogen bath gas (260–1,010 mbar) pressures (*SI Text*, Table S1). A broadband radiation source (150-W Xe arc lamp) was used to excite SO_2 to the mixed $\tilde{A}^1A_2/\tilde{B}^1B_1$ manifold. A 250-nm longpass filter was used to avoid photochemistry from the higher-energy photolysis band ($\tilde{C}^1B_2 \leftarrow \tilde{X}^1A_1$) of SO_2. Photochemistry of SO_2 in the photoexcitation band was studied previously and showed rapid quenching of singlet SO_2 by bath gas (e.g., N_2, CO_2) and reaction of the resulting triplet SO_2 with CO, SO_2, and organic molecules (see ref. 20) (Fig. 1). Experiments were carried out in the presence of acetylene (10 mbar), which efficiently reacts with triplet-state SO_2 (35) and produces organosulfur aerosols, previously characterized as $(C_3H_4S_2O_3)_3$ (36). These were captured and analyzed for quadruple sulfur isotope ratios using techniques described in Oduro et al. (37) and Ono et al. (26).

Results of Photochemical Experiments

All experiments produced organosulfur compounds that had minor fractionations in ^{34}S ($-7.0‰ < \delta^{34}S < 20.8‰$), but were highly enriched in both ^{33}S and ^{36}S ($9.1‰ < \delta^{33}S < 87.3‰$ and $13.8‰ < \delta^{36}S < 135.7‰$) (Table S1 and Fig. 2). This resulted in positive $\Delta^{33}S$ (11.9–77.8‰) and $\Delta^{36}S$ (24.3–109.8‰) values, and positive $\Delta^{36}S/\Delta^{33}S$ ratios of 1.12–2.25. With the exception of our lowest pSO_2 experiment (0.1 mbar), experiments at lower SO_2 pressures produced higher $\Delta^{33}S$ and $\Delta^{36}S$ values than experiments at higher SO_2 pressures under the range of conditions studied, suggesting isotopologue self-shielding is not the dominant source of observed S-MIF anomaly. The sensitivity to pSO_2 might reflect energy transfer between mass-independently fractionated singlet or triplet-state SO_2 and mass-dependently fractionated ground-state SO_2. Such energy transfer might dilute the MIF signal by exciting non-MIF SO_2 into the reactive triplet state. In addition to pSO_2 dependence, $\Delta^{33}S$ values increased as total pressure decreased for experiments run at the same SO_2 pressure. $\Delta^{36}S/\Delta^{33}S$ ratios were sensitive to the total pressure of the system, with higher values (1.98–2.25) at the highest pressure tested (1,013 mbar) and lower values (1.12–1.27) at the lowest pressure (253 mbar) (Fig. 2*A*). These results, particularly the positive $\Delta^{36}S$ and $\Delta^{33}S$ values and small $\delta^{34}S$ values, are consistent with the previous experiments (25) performed with pure SO_2 without N_2 or C_2H_2, suggesting that the observed isotope signature is characteristic of this absorption band system and not a result of the N_2 or C_2H_2 used in the experiment.

To test the sensitivity of the isotope effects to the detailed spectral regions of the excitation, experiments were performed with a series of longpass (250-, 295-, and 305-nm) and shortpass (300- and 350-nm) filters (Fig. S1). The use of optical filters allows testing for S-MIF signals from the high- or low-energy side of the band system (Fig. 1). Experiments performed at the same SO_2 pressure (10 mbar) and total pressure (507 mbar) conditions but with different filters to isolate the 250–300-nm, >295-nm, or >305-nm regions produced remarkably similar isotopic results, with $\Delta^{33}S$ between 30‰ and 36‰ and $\Delta^{36}S$ between 49‰ and 66‰ (Fig. 2*B*). This result suggests that the anomalous enrichment in ^{33}S and ^{36}S is not a strong function of excitation wavelength within this absorption band, at least within a broadband regime. Several experiments were performed with 320-nm longpass and 350-nm shortpass filters. This wavelength region corresponds to excitation into the $\tilde{A}^1A_2$ state only; it is below the origin of the $\tilde{B}^1B_1$ state (38) and above the spin-forbidden $\tilde{a}^3B_1 \leftarrow \tilde{X}^1A_1$ transition of SO_2, which lies between 350 and 390 nm (see references in ref. 20). The experiments were carried out at higher SO_2 (50.7 mbar) and acetylene (101 mbar) pressures, but the same total pressure (507 mbar). These produced lower $\Delta^{33}S$ (11.9–13.5‰) and $\Delta^{36}S$ (24.3–28.0‰) values, consistent with the higher SO_2 pressure, but with $\Delta^{36}S/\Delta^{33}S$ values (2.05–2.08) similar to the rest of the filter experiments (1.61–1.95) (Fig. 2). The presence of S-MIF signatures from excitation exclusively

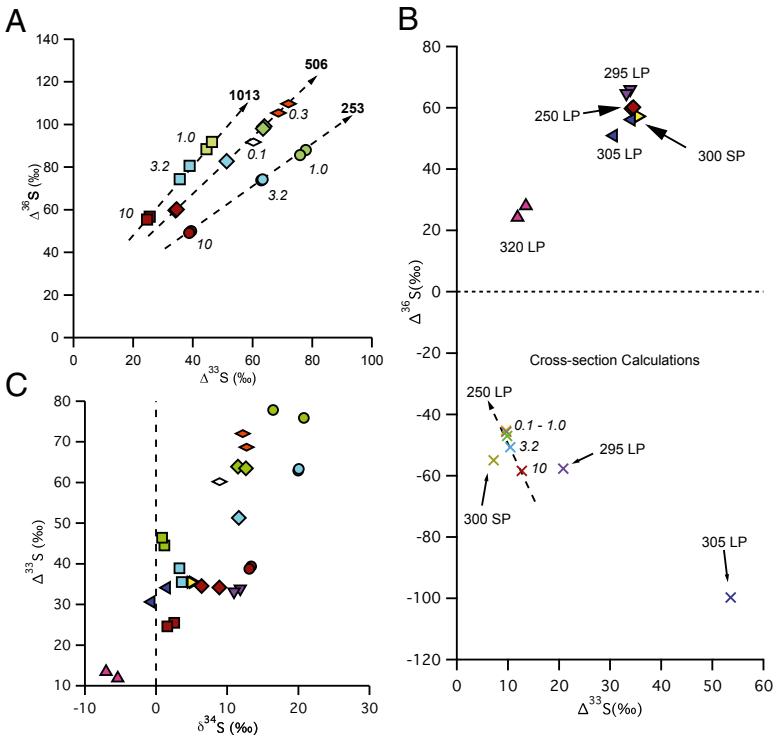

Fig. 2. Isotopic results from experiments and calculations. (*A*) Results ($\Delta^{36}S$ vs. $\Delta^{33}S$) from experiments using the 250-nm longpass filter for a variety of SO_2 pressures (italics, in millibars) and total pressures (bold, in millibars). (*B*) Results ($\Delta^{36}S$ vs. $\Delta^{33}S$) from experiments using various combinations of shortpass (SP) and longpass (LP) filters. The 320 LP experiments also used a 350 SP filter, and the 300 SP experiments also used a 250 LP filter. Also in the figure (× symbols) are the results from calculations based on the Danielache et al. (27) cross-sections for the conditions tested here. (*C*) Results ($\Delta^{33}S$ vs. $\delta^{34}S$) from all experiments, showing the large $\Delta^{33}S$ values associated with small $\delta^{34}S$ values. Symbols are the same as in *A* and *B*.

into the $\tilde{A}^1A_2$ state suggests that vibronic interactions between the two singlet states ($\tilde{B}^1B_1$ and $\tilde{A}^1A_2$) make a negligible contribution to the observed S-MIF signatures.

Source of MIF Signatures

Danielache et al. (27) reported UV cross-sections for isotopically enriched SO_2 (i.e., $^{32}SO_2$, $^{33}SO_2$, $^{34}SO_2$, and $^{36}SO_2$) in the 250–320-nm region. These cross-sections are measured at 8-cm^{-1} resolution, at room temperature, and ∼1–7 mbar SO_2, and characterize the magnitude of the isotopic shifts in band positions and intensities. The measured cross-sections (27) were used to predict S-MIF signatures under the experimental conditions (spectral irradiance and SO_2 column densities) tested here and are compared with experimental results in Fig. 2*B*. The results show that differences in the absorption cross-sections can account for only a small fraction (<25‰) of the large (up to 78‰) $\Delta^{33}S$ values observed in the 250-nm longpass experiments and cannot account for the large positive $\Delta^{36}S$ values (up to 110‰) observed. In particular, the cross-sections predict large negative $\Delta^{36}S$ values for a variety of broadband light sources (Fig. 2*B* and figure 7 in ref. 27), in contrast to the large positive values observed. Even accounting for the systematic errors (2.5%) and SEM (5–10%) for the measured cross-sections (see results and discussion in ref. 27), the cross-sections still cannot explain the $\Delta^{36}S$ values observed (Fig. 2*B*).

The above cross-section model also includes the effect of self- and mutual-shielding of absorption lines under experimental conditions. Self-shielding occurs when the major isotopologue line (i.e., $^{32}SO_2$) saturates under optically thick conditions. In this study, large S-MIF signatures are observed even under optically thin conditions. The experiments with the lowest pSO_2 (column density of 4×10^{16} molecules per cm^{-2}) had over 95% optical transmission, where self-shielding is not expected to play a major role. The magnitude of S-MIF increases with decreasing SO_2 pressure, which is opposite from what is expected from self-shielding. We therefore exclude absorption-based effects, such as self-shielding or absorption cross-section differences as the main source of the observed S-MIF signatures.

Other proposed mechanisms of MIF production include nuclear field shift isotope effects, magnetic isotope effects, and symmetry-based isotope effects. The magnitude of nuclear field shift isotope effects has been estimated to be insignificant for the sulfur isotope system because of the small nuclear size difference among isotopologues (39). Magnetic isotope effects would produce anomalies only in ^{33}S and cannot explain the large $\Delta^{36}S$ values observed in the experiments. A symmetry-based isotope effect also is unlikely because of the lack of any intermediates or transition states with symmetrically equivalent sulfur atoms. In addition, a symmetry-based isotope effect would predict positive $\Delta^{33}S$ values and negative $\Delta^{36}S$ values (40), whereas positive $\Delta^{33}S$ and positive $\Delta^{36}S$ values are observed in the present experiments.

Intersystem Crossing as a Potential Origin of S-MIF

Although isotope substitution shifts the vibrational and rotational energy level spacing in a mass-dependent manner, the magnitudes of the shifts will be different for different excited electronic states. In systems in which the vibration–rotation levels of multiple low-lying electronic states overlap, the interactions between states may exhibit strong and level-specific isotope selectivity. In particular, pairs of levels capable of interacting with each other and that are near-degenerate for one isotopologue may be nondegenerate for other isotopologues. These effects were cited previously as a source of S-MIF during the photopolymerization of CS_2 (41, 42) and oxygen MIF during the photodissociation of CO_2 (43) and CO (44). In these three cases, the anomalous isotope effects have been attributed to differences in intersystem crossing (ISC) rates from an initially excited singlet state to a reactive (or dissociative) triplet state. Similar spin–orbit effects have been shown to cause anomalous LIF intensities in $^{37}ClO_2$ vs. $^{35}ClO_2$ for particular vibrational bands (45). A recent study by Muskatel et al. (46) demonstrates a theoretical basis for similar isotope effects during the photolysis of N_2. In particular, they note that the accidental overlap between different electronic states of N_2 may cause large isotope effects in certain regions of the spectrum. The importance of accidental degeneracies between interacting states in producing environmentally relevant MIF signatures remains controversial,

as it has been suggested that self-shielding might have contributed to the isotope signatures observed during the CS_2 (47) and CO (48–50) (see also ref. 51) experiments. In addition, isotope effects from local interactions are likely to be isolated to narrow spectral regions where the interactions occur.

Several previous spectroscopic studies of SO_2 showed isotopologue-specific perturbations in the 250–350-nm absorption region. Analysis of several absorption bands of $S^{18}O_2$ corresponding to the Clements "B" and "E" bands (310.9 and 304.4 nm, respectively) revealed that these bands of $S^{18}O_2$ were significantly less perturbed than the corresponding bands of $S^{16}O_2$ (52), suggesting different coupling strengths for the different isotopologues. Baskin et al. (53) reported a strong $^{32}SO_2$ vibrational peak at 30,995 cm^{-1} (322.6 nm) that had no corresponding $^{34}SO_2$ peak at the expected location. This was attributed to perturbations caused by accidentally near-degenerate vibronic interactions in one isotopic species but not the other.

If the anomalous isotope effects were purely the result of isolated interactions at particular vibrational levels, a strong wavelength selectivity to the anomalous isotope effects would be expected, with certain regions (i.e., around the localized near-degeneracies) producing considerably larger MIF than other regions. One of the features of the present experiments is that the MIF signature shows remarkable similarity in both the higher- (250–300-nm) and lower- (295–350-nm and 305–350-nm) energy regions of the absorption band (Figs. 1 and 2*B*). Experiments isolating only the 320–350-nm absorption region, which lies below the origin of the $\tilde{B}^1B_1$ state and corresponds to excitation into only the $\tilde{A}^1A_2$ state, also produce S-MIF consistent with the other experiments, although with a smaller magnitude, because of the different experimental conditions (i.e., higher SO_2 pressure).

All our experiments were performed at relatively high total pressures (253–1,013 mbar) in the presence of a bath gas (N_2). Under these conditions, the collision lifetime (on the order of nanoseconds) is considerably shorter than the fluorescence lifetime (on the order of microseconds), allowing rapid collision-induced rotational and vibrational relaxation of the excited state (20, 54). Time-resolved fluorescence experiments performed at 1.33 mbar pure SO_2 showed strong resonance fluorescence from the excited level accompanied by significant fluorescence from vibrationally relaxed molecules (55). At higher SO_2 pressures of 26.6 mbar, fluorescence from highly excited states (266 nm) contained no resonance fluorescence, with the dominant fluorescence occurring around 325.5 nm and 370 nm, near the origin of the $\tilde{B}^1B_1$ and $\tilde{A}^1A_2$ states, respectively, suggesting rapid and nearly complete collisional vibrational thermalization (56). Although the collision-induced ISC might occur from any state, the rate of collision-induced vibrational relaxation is faster than the rate of collision-induced ISC (55), at least for some states. Thus, at high bath gas pressures, the ISC reaction more likely will occur from lower vibrational levels of the singlet state. This also increases the likelihood of vibrational relaxation of the $\tilde{a}^3B_1$ state below the origin of the $\tilde{A}^1A_2$ state, preventing crossing back to the singlet manifold. As a result, localized near-degenerate interactions at low vibrational levels of the singlet state will be selectively expressed regardless of the state and vibrational levels initially excited into. This allows a mechanism for the expression of S-MIF from localized near-degenerate spin–orbit interactions, and also may explain the pressure dependence on the relationship between $\Delta^{36}S$ and $\Delta^{33}S$ values.

Theoretical Basis for Proposed Mechanism

To better understand the isotope effects during the ISC reaction of SO_2, high-level ab initio calculations of the global potential energy surfaces (PESs) for the low-lying singlet and triplet states of SO_2 were carried out (*SI Text*). In the Clements bands (57), about 3.5 eV above the ground electronic ($\tilde{X}^1A_1$) state, there are two nonadiabatically coupled singlet ($\tilde{A}\ ^1A_2$ and $\tilde{B}\ ^1B_1$) and three triplet ($\tilde{a}^3B_1$, $\tilde{b}^3A_2$, and $\tilde{c}^3B_2$) electronic states (58–60) (Fig. 2*D*). The $\tilde{c}^3B_2$ state was not included in the present analysis, as it has no interaction with other states because of its symmetry. For each of the remaining states, ~19,000 symmetric unique points were determined at the internally contracted multireference configuration interaction (MRCI) level (61) with the augmented correlation-consistent polarized valence triple-zeta (aug-cc-pVTZ) basis set (62) for both the sulfur and oxygen atoms. The Davidson correction (Q) (63) was applied to account for the effect of higher excitations and to reduce size-consistency errors. Nonadiabatic couplings between the two singlet states have been determined in a quasi-diabatic representation (64). In addition, the spin–orbit (SO) interactions between the singlet and triplet states has been computed using the unperturbed MRCI wave functions and Breit–Pauli Hamiltonian. As shown in *SI Text* (Fig. S2), the calculated absorption cross-section for the Clements bands is in good agreement with experiment. Importantly, the potential energy minimum of the $\tilde{a}^3B_1$ state is about 0.2 eV lower than that of the lowest singlet state, facilitating ISC.

Franck–Condon transitions with a 250–350-nm photon bring SO_2 from the ground $\tilde{X}^1A_1$ state to the excited $\tilde{A}^1A_2/\tilde{B}^1B_1$ manifold. As discussed above, we assume that the excited SO_2 is relaxed quickly to low vibrational levels (Table S2) of the lowest singlet $\tilde{A}^1A_2$ state because of fast nonadiabatic mixing between the two singlet states and efficient collisions with the bath gas. The ISC to the lowest triplet $\tilde{a}^3B_1$ state follows (Table S2), which was modeled using a wave packet method. In particular, the time-dependent Schrödinger equation was solved numerically (65) with the nonadiabatically coupled full-dimensional Hamiltonian for the $\tilde{B}^1B_1/\tilde{A}^1A_2/\tilde{a}^3B_1$ manifold ($J = 0$), as described in *SI Text*. Four (000, 100, 010, and 001) vibrational eigenfunctions on the $\tilde{A}^1A_2$ state were used as the initial wave packet, and the $\tilde{a}^3B_1$ triplet-state population is artificially absorbed to account for the irreversibility of the ISC as a result of collisional relaxation. The parameters used in our calculations are listed in Table S3.

The lifetime of the $\tilde{A}^1A_2$ state is extracted from the population decay curve (Table S4) and used to estimate the isotope effects for ISC from each vibrational level. As shown in Fig. 3 and Fig. S3, the results clearly show the decay rates are different among the sulfur isotopologues and are not mass dependent. In particular, the (000), (100), and (001) vibrational levels show large anomalies in the decay rate of $^{36}SO_2$, suggesting a strong mass-independent effect in ^{36}S. Similarly, decay from the (010) level shows large MIF in ^{33}S. Therefore, combined contributions from MIF at the (100) and (010) levels would explain the experimental results of positive $\Delta^{33}S$ and $\Delta^{36}S$ values. It is clear that this simple model cannot fully account for the experimental results; a significant number of approximations were involved. For example, the relative energies of various electronic states might not be determined accurately by the ab initio method. In addition, it is likely that the singlet excited-state SO_2 decays from a range of vibrational and rotational levels. Nevertheless, these results clearly demonstrate that there is a very strong, isotope-specific dependence on the excited-state lifetimes from individual vibrational levels.

Implications to S-MIF Signatures Observed in Nature

The photolysis of SO_2 in the 185–220-nm absorption region currently is considered the most likely source reaction for Archean S-MIF (18, 19, 22–24). However, there are several issues with SO_2 photolysis as a source of the Archean S-MIF signatures. Broadband photolysis of SO_2 under a range of experimental conditions (e.g., SO_2 pressures, bath gas pressures, light sources) produces large $\delta^{34}S$ values (up to 212‰) associated with relatively small $\Delta^{33}S$ enrichments (maximum 25‰), resulting in low $\delta^{33}S/\delta^{34}S$ ratios of 0.55–0.66 (24–26). In contrast, the Archean record contains large $\Delta^{33}S$ values (from −4 to +12 ‰) associated with high $\delta^{33}S/\delta^{34}S$ ratios of up to 1.4 (e.g., refs. 66 and 67). In addition, S-MIF signatures produced during SO_2 photolysis become

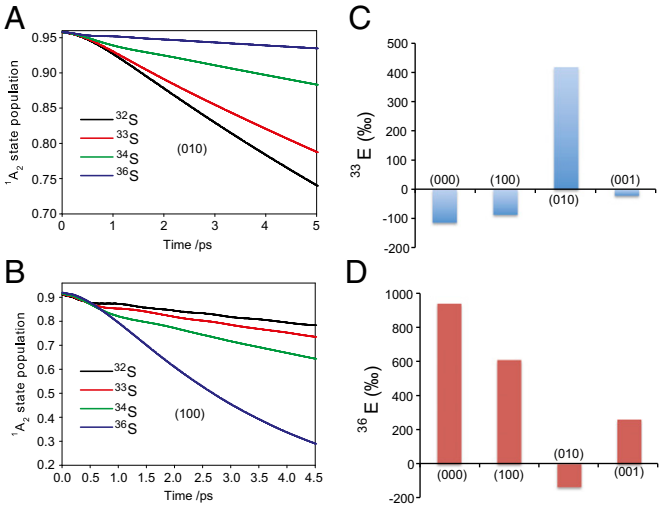

Fig. 3. Results for lifetime calculations for $\tilde{A}^1A_2$ states. (*A* and *B*) Decay of singlet populations for several sulfur isotopologues from the (010) and (100) vibrational states, which have rates faster than those of the (000) and (001) states (Table S4). (*C* and *D*) Isotope fractionation factor estimated from the lifetime of $\tilde{A}^1A_2$ state calculated for the four low-lying vibrational levels: $^{33}E = (^{33}k/^{32}k)/(^{34}k/^{32}k)^{0.515} - 1$, and $^{36}E = (^{36}k/^{32}k)/(^{34}k/^{32}k)^{1.9} - 1$, where ^{x}k are rate constants for $^{x}SO_2$.

very small ($\Delta^{33}S < 2.5‰$) at low SO_2 column densities (26), indicating that the production of large ($\Delta^{33}S > 2.5‰$) S-MIF anomalies would require the maintenance of high SO_2 column densities in the atmosphere. Sediment digenesis and biological processes in the oceans likely mix sulfides with different $\Delta^{33}S$ values and dilute the S-MIF signal (68) such that the source reaction likely would have produced $\Delta^{33}S$ values much larger than 12‰. Significant questions remain as to whether 185–220-nm photolysis of SO_2 was the source of Archean S-MIF.

The S-MIF signatures produced in this study contain large ($\Delta^{33}S$ up to 78‰) MIF associated with small (<25‰) $\delta^{34}S$ values. In contrast to the photolysis band, the S-MIF signatures from the excitation band do not require a high SO_2 column density to produce large S-MIF. The major issues with the excitation band as a source of the Archean S-MIF signature are the difficulty in preserving the isotope signatures from excited-state SO_2 (relative to SO produced from SO_2 photolysis) and the positive $\Delta^{36}S/\Delta^{33}S$ ratios (Archean rocks have $\Delta^{36}S/\Delta^{33}S$ ~−1.5 to −0.9; see refs. 15, 32, and 67). Several authors (25, 32) have suggested that SO_2 photochemistry from the photoexcitation region might have contributed to the Archean S-MIF signatures, and studies have shown that the UV irradiation of SO_2 in the presence of methane produces organosulfur aerosols (presumably derived from $^3SO_2$) that might have contributed to preservation of the Archean S-MIF signature (69). The discrepancy in $\Delta^{36}S/\Delta^{33}S$ values requires additional study, but our calculations suggest that MIFs in ^{33}S and ^{36}S are produced from ISC at different vibrational levels, and our experiments demonstrated that the $\Delta^{36}S/\Delta^{33}S$ ratio is a function of pN_2 and could potentially produce the Archean ratio under certain conditions. It should be noted that the $\Delta^{36}S/\Delta^{33}S$ values produced from experimental photolysis of SO_2 using broadband radiation sources is too low (−1.6 under pure SO_2 but as low as −6.0 with N_2) to explain the $\Delta^{36}S/\Delta^{33}S$ ratios observed for the Archean record. As suggested in Whitehill and Ono (25), contributions from both absorption regions might explain the Archean S-MIF signal.

Several authors (e.g., refs. 28–31) have suggested that excited-state photochemistry in the photoexcitation band might be responsible for the S-MIF signatures observed in modern stratospheric sulfate aerosols. Reaction of excited-state SO_2, particularly triplet $^3SO_2$, with either ground-state SO_2 [i.e., $^*SO_2+SO_2 \rightarrow SO+SO_3$ (29)] or O_2 [i.e., $^*SO_2+O_2 \rightarrow SO_3+O$ (28)] theoretically could preserve mass-independently fractionated SO_3, and SO_3 might be hydrolyzed to form stable sulfuric acid aerosols. Whitehill and Ono (25), however, presented isotopic evidence that the $^*SO_2+SO_2$ reaction primarily occurs via O-atom transfer from the excited-state species to the ground-state species, thus producing MIF signatures in SO, but mass-dependently fractionated SO_3. Hattori et al. (28) modeled the modern stratosphere following a large volcanic eruption and suggested that the $^*SO_2$ formed from the photoexcitation band might react with O_2 to form mass-independently fractionated SO_3 (29–31). Their isotopic agreement, however, critically depends on the assumption that the cross-sections of Danielache et al. (27) accurately predict the isotope ratios of the reactive (i.e., triplet) SO_2 species. As we demonstrate here, significant differences between the isotope signatures predicted by the cross-sections and those observed experimentally are the result of vibronic effects after the initial excitation step, which are not taken into account in ref. 28. Ono et al. (26) showed that the isotopic signatures from SO_2 photolysis in a self-shielding regime match those from stratospheric sulfate aerosols, although a mechanism for the preservation of SO in the modern atmosphere requires additional research.

Conclusions

We report the production of very large S-MIF signatures, with $\Delta^{33}S$ up to 78‰ and $\Delta^{36}S$ up to 110‰, from SO_2 photochemistry in the 250–350-nm region. The origin of the S-MIF is attributed to ISC at excitation wavelengths below 320 nm. Isotope effects due primarily to absorption, as predicted by isotopologue-specific cross-sections, do not contribute significantly to the large S-MIF observed, particularly in ^{36}S. Rapid vibrational relaxation allows expression of S-MIF signatures from localized accidental degeneracies regardless of the initially excited vibronic level. The same mechanism, however, may not be applied to the 180- and 220-nm band systems of SO_2 because the quantum efficiency of photolysis is near unity below 205 nm (59), and the lifetime is sufficiently short that little vibrational relaxation occurs. Although the S-MIF signatures observed in this study, particularly the $\Delta^{36}S/\Delta^{33}S$ ratios, do not match those from the Archean, the photochemistry in the photoexcitation band can produce large mass-independent signatures (i.e., $\Delta^{33}S$ values) with relatively small mass-dependent fractionations (i.e., $\delta^{34}S$ values), which is necessary to explain the preservation of large Archean S-MIF signatures. Photochemistry from the 250–350-nm absorption region should be explored further as a possible source for the geological S-MIF signatures.

ACKNOWLEDGMENTS. The authors thank William J. Olszewski for assistance in sulfur isotope analysis, and Harry Oduro and Eliza Harris for discussion. The authors also thank Robert Field for his input and suggestions. This work was supported by the National Aeronautics and Space Administration Exobiology Program, Grant NNX10AR85G (to S.O.); the National Natural Science Foundation of China (21133006, 91221301, and 91021010); the Ministry of Science and Technology (2013CB834601 to D.X.); and the Department of Energy, Grant DF-FG02-05ER15694 (to H.G.).

1. Urey HC (1947) The thermodynamic properties of isotopic substances. *J Chem Soc* 69: 562–581.
2. Bigeleisen J, Mayer M (1947) Calculation of equilibrium constants for isotopic exchange reactions. *J Chem Phys* 15(5):261–267.
3. Thiemens MH (1999) Mass-independent isotope effects in planetary atmospheres and the early solar system. *Science* 283(5400):341–345.
4. Thiemens M (2006) History and applications of mass-independent isotope effects. *Annu Rev Earth Planet Sci* 34:217–262.

5. Thiemens MH, Chakraborty S, Dominguez G (2012) The physical chemistry of mass-independent isotope effects and their observation in nature. *Annu Rev Phys Chem* 63:155–177.
6. Hulston J, Thode H (1965) Variations in the S^{33}, S^{34}, and S^{36} contents of meteorites and their relation to chemical and nuclear effects. *J Geophys Res* 70(14):3475–3484.
7. Clayton RN, Grossman L, Mayeda TK (1973) A component of primitive nuclear composition in carbonaceous meteorites. *Science* 182(4111):485–488.
8. Arrhenius G, McCrumb J, Friedman N (1979) Primordial condensation of meteorite components—experimental evidence of the state of the medium. *Astrophys Space Sci* 65:297–307.
9. Thiemens MH, Heidenreich JE, 3rd (1983) The mass-independent fractionation of oxygen: A novel isotope effect and its possible cosmochemical implications. *Science* 219(4588):1073–1075.
10. Thiemens M, Jackson T (1987) Produciton of isotopically heavy ozone by ultraviolet light photolysis of O_2. *Geophys Res Lett* 14(6):624–627.
11. Mauersberger K (1987) Ozone isotope measurements in the stratosphere. *Geophys Res Lett* 14(1):80–83.
12. Mauersberger K, Krankowsky D, Janssen C, Schinke R (2005) Assessment of the ozone isotope effect. *Advances in Atomic, Molecular, and Optical Physics*, eds Bederson B, Walther H (Elsevier, Amsterdam), Vol 50, pp 1–54.
13. Schinke R, Grebenshchikov SY, Ivanov MV, Fleurat-Lessard P (2006) Dynamical studies of the ozone isotope effect: A status report. *Annu Rev Phys Chem* 57:625–661.
14. Ivanov MV, Babikov D (2013) On molecular origin of mass-independent fractionation of oxygen isotopes in the ozone forming recombination reaction. *Proc Natl Acad Sci USA* 110:17708–17713.
15. Farquhar J, Bao H, Thiemens M (2000) Atmospheric influence of Earth's earliest sulfur cycle. *Science* 289(5480):756–759.
16. Bekker A, et al. (2004) Dating the rise of atmospheric oxygen. *Nature* 427(6970): 117–120.
17. Guo Q, et al. (2009) Reconstructing Earth's surface oxidation across the Archean-Proterozoic transition. *Geology* 37(5):399–402.
18. Farquhar J, Savarino J, Airieau S, Thiemens M (2001) Observation of wavelength-sensitive mass-independent sulfur isotope effects during SO_2 photolysis: Implications for the early atmosphere. *J Geophys Res* 106(E12):32829–32839.
19. Pavlov AA, Kasting JF (2002) Mass-independent fractionation of sulfur isotopes in Archean sediments: Strong evidence for an anoxic Archean atmosphere. *Astrobiology* 2(1):27–41.
20. Heicklen J, Kelly N, Partymiller K (1980) The photophysics and photochemistry of SO_2. *Res Chem Intermed* 3:315–404.
21. Ran H, Xie D, Guo H (2007) Theoretical studies of $\tilde{C}^1B_2$ absorption spectra of SO2 isotopomers. *Chem Phys Lett* 439:280–283.
22. Lyons J (2007) Mass-independent fractionation of sulfur isotopes by isotope-selective photodissociation of SO_2. *Geophys Res Lett* 34:L22811.
23. Danielache S, Eskebjerg C, Johnson M, Ueno Y, Yoshida N (2008) High-precision spectroscopy of ^{32}S, ^{33}S, and ^{34}S sulfur dioxide: Ultraviolet absorption cross sections and isotope effects. *J Geophys Res* 113:D17314.
24. Masterson A, Farquhar J, Wing B (2011) Mass-independent fractionation patterns in the broadband UV photolysis of sulfur dioxide: Pressure and third body effects. *Earth Planet Sci Lett* 306:253–260.
25. Whitehill A, Ono S (2012) Excitation band dependence of sulfur isotope mass-independent fractionation during photochemistry of sulfur dioxide using broadband light sources. *Geochim Cosmochim Acta* 94:238–253.
26. Ono S, Whitehill A, Lyons J (2013) Contribution of isotopologue self-shielding to sulfur mass-independent fractionation during sulfur dioxide photolysis. *J Geophys Res Atmos* 118(5):2444–2454.
27. Danielache S, et al. (2012) Photoabsorption cross-section measurements of 32S,33S, 34S, and 36S sulfur dioxide for the B^1B_1–X^1A_1 absorption band. *J Geophys Res Atmos* 117(D24):D24301.
28. Hattori S, et al. (2013) SO_2 photoexcitation mechanism links mass-independent sulfur isotopic fractionation in cryospheric sulfate to climate impacting volcanism. *Proc Natl Acad Sci USA* 110:17656–17661.
29. Savarino J, Romero A, Cole-Dai J, Bekki S, Thiemens M (2003) UV induced mass-independent sulfur isotope fractionation in stratospheric volcanic sulfate. *Geophys Res Lett* 30(21):2131.
30. Baroni M, Thiemens MH, Delmas RJ, Savarino J (2007) Mass-independent sulfur isotopic compositions in stratospheric volcanic eruptions. *Science* 315(5808):84–87.
31. Baroni M, Savarino J, Cole-Dai J, Rai V, Thiemens M (2008) Anomalous sulfur isotope compositions of volcanic sulfate over the last millennium in Antarctic ice cores. *J Geophys Res* 113:D20112.
32. Zerkle A, Claire M, Domagal-Goldman S, Farquhar J, Poulton S (2012) A bistable organic-rich atmosphere on the Neoarchaean Earth. *Nat Geosci* 5:359–363.
33. Vandaele A, Hermans C, Fally S (2009) Fourier transform measurements of SO_2 absorption cross sections: II.: Temperature dependence in the 29000–44000 cm^{-1} (227–345 nm) region. *J Quant Spectrosc Radiat Transf* 110(18):2115–2126.
34. Hermans C, Vandaele A, Fally S (2009) Fourier transform measurements of SO_2 absorption cross sections: I. Temperature dependence in the 24000 – 29000 cm^{-1} (345 – 420 nm) region. *J Quant Spectrosc Radiat Transf* 110:756–766.
35. Kelly M, Meagher J, Heicklen J (1976) Photolysis of sulfur dioxide in the presence of foreign gases: VII. Acetylene. *J Photochem* 5:355–376.
36. Luria M, de Pena R, Olszyna K, Heicklen J (1974) Kinetics of particle growth. III. Particle formation in the photolysis of sulfur dioxide–acetylene mixtures. *J Phys Chem* 78(4): 325–335.
37. Oduro H, Kamyshny A, Guo W, Farquhar J (2011) Multiple sulfur isotope analysis of volatile organic sulfur compounds and their sulfonium precursors in coastal marine environments. *Mar Chem* 124:78–89.
38. Shaw R, Kent J, O'Dwyer M (1980) Single vibronic level fluorescence spectra of sulfur dioxide. *J Mol Spectrosc* 82(1):1–26.
39. Schauble E (2007) Role of nuclear volume in driving equilibrium stable isotope fractionation of mercury, thallium, and other very heavy elements. *Geochim Cosmochim Acta* 71:2170–2189.
40. Ono S, Beukes N, Rumble D (2009) Origin of two distinct multiple-sulfur isotope compositions of pyrite in the 2.5 Ga Klein Naute Formation, Griqualand West Basin, South Africa. *Precambrian Res* 169(1-4):48–57.
41. Colman JJ, Xu X, Thiemens MH, Trogler WC (1996) Photopolymerization and mass-independent sulfur isotope fractionations in carbon disulfide. *Science* 273(5276): 774–776.
42. Zmolek P, Xu X, Jackson T, Thiemens M, Trogler W (1999) Large mass independent sulfur isotope fractionations during the photopolymerization of $^{12}CS_2$ and $^{13}CS_2$. *J Phys Chem A* 103(15):2477–2480.
43. Bhattacharya S, Savarino J, Thiemens M (2000) A new class of oxygen isotopic fractionation in photodissociation of carbon dioxide: Potential implications for atmospheres of Mars and Earth. *Geophys Res Lett* 27(10):1459–1462.
44. Chakraborty S, Ahmed M, Jackson TL, Thiemens MH (2008) Experimental test of self-shielding in vacuum ultraviolet photodissociation of CO. *Science* 321(5894): 1328–1331.
45. Lim G, Lim S, Kim S, Choi Y (1999) Unexpectedly large $O^{37}ClO/O^{35}ClO$ intensity ratios of the fluorescence from the low-energy vibrational levels of OClO ($\tilde{A}^2A_2$). *J Chem Phys* 111:456–459.
46. Muskatel BH, Remacle F, Thiemens MH, Levine RD (2011) On the strong and selective isotope effect in the UV excitation of N_2 with implications toward the nebula and Martian atmosphere. *Proc Natl Acad Sci USA* 108(15):6020–6025.
47. Lyons J (2009) Atmospherically-derived mass-independent sulfur isotope signatures, and incorporation into sediments. *Chem Geol* 267:164–174.
48. Lyons J, Lewis R, Clayton R (2009) Comment on "Experimental test of self-shielding in vacuum ultraviolet photodissociation of CO." *Science* 324(5934):1516.
49. Federman S, Young E (2009) Comment on "Experimental test of self-shielding in vacuum ultraviolet photodissociation of CO." *Science* 324(5934):1516.
50. Yin QZ, Shi X, Chang C, Ng CY (2009) Comment on "Experimental test of self-shielding in vacuum ultraviolet photodissociation of CO." *Science* 324(5934):1516, author reply 1516.
51. Chakraborty S, Ahmed M, Jackson T, Thiemens M (2009) Response to comments on "Experimental test of self-shielding in vacuum ultraviolet photodissociation of CO." *Science* 324(5934):1516.
52. Hamada Y, Merer A (1975) Rotational structure in the absorption spectrum of SO_2 between 3000 Å and 3300 Å. *Can J Phys* 53:2555–2576.
53. Baskin J, Al-Adel F, Hamden A (1995) Unexpectedly rich vibronic structure in supersonic jet spectra of sulfur dioxide between 360 and 308 nm. *Chem Phys* 200:181–199.
54. Su F, et al. (1978) Kinetics of fluorescence decay of SO_2 excited in the 2662–3273 Å region. *Int J Chem Kinet* 10:125–154.
55. Bae S, Yoo H, Ku J (1998) Intersystem crossing rate constants from the (0,4,1) and (1,2,1) levels of the $\tilde{A}$ $^1A_2$ to $\tilde{a}$ $^1B_1$ state of SO_2. *J Chem Phys* 109(4):1251–1258.
56. Zhang G, Zhang L, Jin Y (2010) Emission spectrum and relaxation kinetics of SO_2 induced by 266 nm laser. *Spectrochim Acta A Mol Biomol Spectrosc* 77(1):141–145.
57. Clements J (1935) On the absorption spectrum of sulphur dioxide. *Phys Rev* 47: 224–232.
58. Müller H, Köppel H (1994) Adiabatic wave-packet motion on conically intersecting potential energy surfaces. The case of SO_2 ($^1B_1$ – $^1A_2$). *Chem Phys* 183:107–116.
59. Katagiri H, et al. (1997) Experimental and theoretical exploration of photodissociation of SO_2 via the C^1B_2 state: Identification of the dissociation pathway. *J Molec Struct* 413:589–614.
60. Lévêque C, Komainda A, Taïeb R, Köppel H (2013) Ab initio quantum study of the photodynamics and absorption spectrum for the coupled $1^{(1)}A_2$ and $1^{(1)}B_1$ states of SO_2. *J Chem Phys* 138(4):044320.
61. Werner H, Knowles P (1988) An efficient internally contracted multiconfiguration-reference configuration interaction method. *J Chem Phys* 89:5803–5814.
62. Dunning T (1989) Gaussian basis sets for use in correlated molecular calculations. I. The atoms boron through neon and hydrogen. *J Chem Phys* 90:1007–1023.
63. Langhoff S, Davidson E (1974) Configuration interaction calculations on the nitrogen molecule. *Int J Quantum Chem* 8(1):61–72.
64. Simah D, Hartke B, Werner H (1999) Photodissociation dynamics of H_2S on new coupled ab initio potential energy surfaces. *J Chem Phys* 111(10):4523–4534.
65. Kosloff R (1988) Time-dependent quantum-mechanical methods for molecular dynamics. *J Phys Chem* 92(8):2087–2100.
66. Ono S, et al. (2003) New insights into Archean sulfur cycle from mass-independent sulfur isotope records from the Hamersley Basin, Western Australia. *Earth Planet Sci Lett* 213:15–30.
67. Kaufman AJ, et al. (2007) Late Archean biospheric oxygenation and atmospheric evolution. *Science* 317(5846):1900–1903.
68. Halevy I, Johnston DT, Schrag DP (2010) Explaining the structure of the Archean mass-independent sulfur isotope record. *Science* 329(5988):204–207.
69. DeWitt HL, et al. (2010) The formation of sulfate and elemental sulfur aerosols under varying laboratory conditions: implications for early earth. *Astrobiology* 10(8): 773–781.